

# Intraseasonal variability of wintertime frontal activity and its relationship with precipitation anomalies in the vicinity of South America

Josefina Blázquez<sup>1</sup> · Silvina A. Solman<sup>1</sup>

Received: 29 October 2014 / Accepted: 6 June 2015 / Published online: 19 June 2015  
© Springer-Verlag Berlin Heidelberg 2015

**Abstract** The intraseasonal variability of the frontal activity and its connection with the variability of the atmospheric circulation and precipitation in the Southern Hemisphere is studied. The frontal activity is defined as the relative vorticity times the local temperature gradient. A band-pass filter was applied to retain the intraseasonal timescales. An empirical orthogonal function analysis was applied to the filtered frontal activity anomalies. The two main modes show positive and negative centers located mainly over the southern Pacific Ocean and South American sector and are in quadrature with each other. A similar pattern was found when the main modes of intraseasonal variability of the 500 hPa geopotential height were projected on the frontal activity, suggesting that the variability of fronts are influenced by the variability of the large scale atmospheric circulation. Moreover, the precipitation anomalies projected on the main modes of both frontal activity and 500 hPa geopotential height show similar structures, especially over the southern Pacific Ocean and South America, which may indicate that the variability of fronts controls the variability of precipitation. The lagged regression of the time series of the frontal activity areally-averaged over one of the centers of action against the frontal activity anomaly field shows at lags  $-8$  and  $8$  a similar

pattern, suggesting a period of around 17 days for each mode. Moreover, lagged regression between times series of frontal activity and precipitation anomalies reveals an opposite pattern between southeastern South America and southern Chile, being precipitation anomalies over these two regions anti-correlated due to the frontal activity.

**Keywords** Frontal activity · Precipitation · Large scale circulation · Intraseasonal variability · Southern Hemisphere

## 1 Introduction

The variability of the atmospheric circulation has been widely studied in the last years. Both at the intraseasonal and interannual timescales, the main modes of variability of the wintertime atmospheric circulation of Southern Hemisphere (SH) are the Pacific South America modes (PSAs) and the southern annular mode (SAM). In particular at the intraseasonal timescale, Mo and Ghil (1987) and later Ghil and Mo (1991) identified the PSAs patterns, which consist in a wave train that emanates from the equatorial Pacific and propagates poleward in the SH. Furthermore, the SAM was also fully documented at this timescale (Kidson 1988; Thompson and Wallace 2000; among others). This mode exhibits a wavenumber 1 on high latitudes and a wavenumber 3–4 pattern at mid-latitudes with opposite signs. Therefore, these three patterns are the main structures of circulation variability at the intraseasonal timescales of the SH.

Precipitation variability at the intraseasonal timescale was also fully documented over South America. A distinctive pattern in summer precipitation was reported by Nogués Paegle and Mo (1997). This pattern is known as the South American Seesaw dipole (SASS) and represents

✉ Josefina Blázquez  
blazquez@cima.fcen.uba.ar

Silvina A. Solman  
solman@cima.fcen.uba.ar

<sup>1</sup> Departamento de Ciencias de la Atmósfera y los Océanos (FCEN-UBA), Centro de Investigaciones del Mar y la Atmósfera (CIMA-CONICET/FCEN-UBA), Instituto Franco Argentino del Clima y sus Impactos (UMI IFAECI/CNRS), Ciudad Universitaria Pabellón II Piso 2 (C1428EGA), Buenos Aires, Argentina

the main mode of intraseasonal variability. Recently, Alvarez et al. (2014) have identified the intraseasonal modes of variability for winter of the outgoing longwave radiation (OLR) for southeastern South America (SESA) and found two main modes explaining approximately 34 % of the total variance. The first one shows the main signal in an extended area, which includes Bolivia Paraguay, northern Argentina and southern Brazil, the second displays the main centre over east of Uruguay and south Brazil and another centre of opposite sign extended from the Amazon region to the southeastern Brazil.

It is extensively known that the precipitation variability over South America is conditioned by the atmospheric circulation variability of the SH; there are numerous studies that confirm this relationship (Mo and Higgins 1998; Liebmann et al. 1999; Cunningham and Cavalcanti 2006; Solman and Orlanski 2010; Gonzalez and Vera 2014; Alvarez et al. 2014; among others).

On the other hand, it is known that precipitation at high and subtropical latitudes of the SH is much related with the frontal activity, especially in austral winter. Fronts are the dynamic mechanism that triggers the convection and thus the subsequent precipitation (Bjerknes and Solberg 1922; Browning and Roberts 1994). Recently, Catto et al. (2012) found that the midlatitudes regions of the SH are one of the regions where most precipitation is associated with fronts. At the regional scale, Pook et al. (2006) showed that 41 % of total precipitation during July over southern Australia is due to frontal activity. Recently, Solman and Orlanski (2014) have documented that the poleward shift of the frontal activity in the SH is consistent with the midlatitudes drying and high-latitude moistening, showing a strong relationship between fronts and precipitation.

Fronts are meteorological systems that are a consequence of the high frequency variability of the atmospheric circulation. In particular, in the SH there are several studies that document this relationship (Kidson and Sinclair 1995; Berbery and Vera 1996; Cavalcanti and Kayano 1999). Moreover, the synoptic scale activity is modulated by low frequency variability patterns. For example Vera (2003) relates the interannual variability of storm-tracks with the low frequency variability patterns. Therefore, knowing the main intraseasonal modes of variability of the atmospheric circulation, the first question that is being addressed in this paper is: how do these patterns condition the fronts in the intraseasonal timescale? Furthermore, fronts and precipitation are much related, so the second question is: how does the variability of frontal activity impact the variability of precipitation?

Considering that frontal activity is the mechanism that controls the precipitation that in turn is conditioned by the atmospheric circulation, the main hypothesis in this study is that at intraseasonal timescales the variability of the large scale circulation controls the variability of the frontal activity

that in turn affect the variability of precipitation. Here, the frontal activity is represented by the cyclonic feature of the frontal system. The main objectives of this paper are: (1) to identify the leading modes of variability of the frontal activity in the western SH; (2) to explore the relationship between the modes of variability of fronts with the modes of variability of the large scale circulation; (3) to explore to what extent the main frontal activity modes of variability affect the precipitation anomalies over southern South America.

This paper is organized as follows: data and methodologies used in this study are presented in Sect. 2. The results are described in Sect. 3. Finally, a summary of the results and main conclusions are discussed in Sect. 4.

## 2 Data and methodology

Daily data from the European Centre Medium Range Weather Forecasts (ECMWF) 40 year Reanalysis (ERA40) (Uppala et al. 2005) with 2.5° of resolution for the period 1979–2001 was used in this study. In particular, geopotential height of 500 hPa, front-index (hereafter FI) and precipitation were used to analyse the variability of atmospheric circulation, frontal activity and precipitation in the SH, respectively. The FI was calculated in all grid points following Solman and Orlanski (2010), as the relative vorticity times the local temperature gradient at 850 hPa:

$$FI = |\nabla T_{850 \text{ hPa}}| \times \xi_{850 \text{ hPa}}$$

Solman and Orlanski (2014) showed that FI represents adequately frontal systems in the SH. Moreover, the authors also remark that the percentage of precipitation associated with fronts ranges between 70 and 80 % at the extratropical latitudes of the SH, in agreement with Catto et al. (2012). Precipitation data from the Climate Prediction Center unified gauge dataset (CPC-uni) (Xie et al. 2007) on a 0.5° grid was also used. The reason for using two different datasets for precipitation is that there is no observed gridded daily dataset covering both oceanic and land areas for the period used in this study. That is why ERA40 reanalysis was used in calculations which involve both ocean and land data, while CPC-uni was used only when land data was required. A comparison between the two precipitation datasets was performed for southern South America. Both ERA40 and CPC-uni agree on the spatial pattern of mean precipitation during the SH winter, with a maximum over SESA and southern Chile (not shown). Additionally, and in order to check for consistency in the variability of rainfall from the two datasets, a power spectrum of the time series of precipitation over the regions where maximum precipitation were identified was calculated and it was found that the two datasets agree on the main features of the spectra (not shown).

This study was performed during austral extended winter: May, June, July and August (MJJJA). Daily anomalies were computed by subtracting the monthly mean climatology from the raw data. In particular, the FI anomalies were calculated using only cyclonic values. Positive (negative) values of FI anomalies indicate more (less) frontal activity than the average, associated with their intensity and/or frequency. Then the anomalies were filtered using a Lanczos filter with 501 daily weights (Duchon 1979) to isolate the intraseasonal timescale retaining periods between 11 and 60 days.

The Empirical Orthogonal Function (EOF) technique was used to detect the leading modes of variability of FI in the SH, from 70°S to 15°S. It is worth to mention that some factors may limit the physical interpretation of EOFs: the domain dependence of the derived patterns (Richman 1986) and the spatial orthogonality of the modes (Hannachi et al. 2007). Therefore, some sensitivity tests were performed to explore the robustness of the leading modes identified, not only with respect to its dependence on the domain size but also to explore the orthogonality problem. First, the EOF of FI was computed over the entire domain; the largest amplitude of the leading modes was located over the western part of HS (not shown). The calculation was repeated over a reduced domain covering the western Hemisphere (180°W to 0°) and the patterns identified were

similar to those found for the large domain. Regarding the orthogonality constraint, the Rotated EOF (REOF) over the reduced domain was also computed and the results were close to those found in the previous analysis. Therefore, the leading modes of the FI were computed for the reduced domain with non-rotated EOFs. The leading modes of the 500 hPa geopotential height anomalies were also computed for the whole SH.

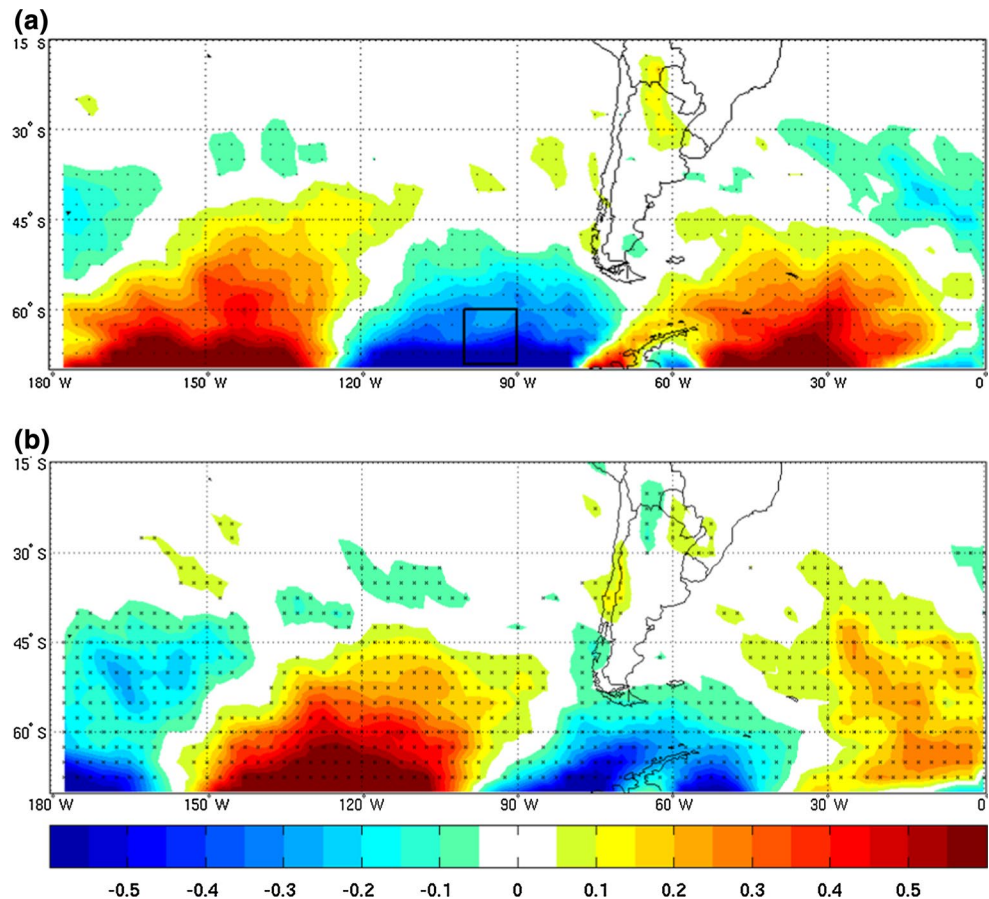
To evaluate the relationships among FI, geopotential height and precipitation anomalies, lagged regressions and correlations were calculated. A Fisher test was implemented to evaluate the statistical significance of the correlation coefficients using 500° of freedom and a confidence level of 95 %. It is worth noting that the number of days in one extended winter (MJJJA) multiplied by 23 years is 2829, however, to avoid dependence of data, the total number of days was divided by five (decorrelation time).

### 3 Results

#### 3.1 Intraseasonal variability patterns of FI

As it was mentioned previously, the main objective of this paper is to analyse how the variability of the frontal activity

**Fig. 1** Regression of the front-index anomaly field against the first (a) and second (b) PCs of front-index calculated with the filtered (11–60 days) anomalies. Dots mean 95 % confidence level, according a Fisher test. Units are  $1.e10 \text{ } ^\circ\text{C m}^{-1} \text{ s}^{-1}$

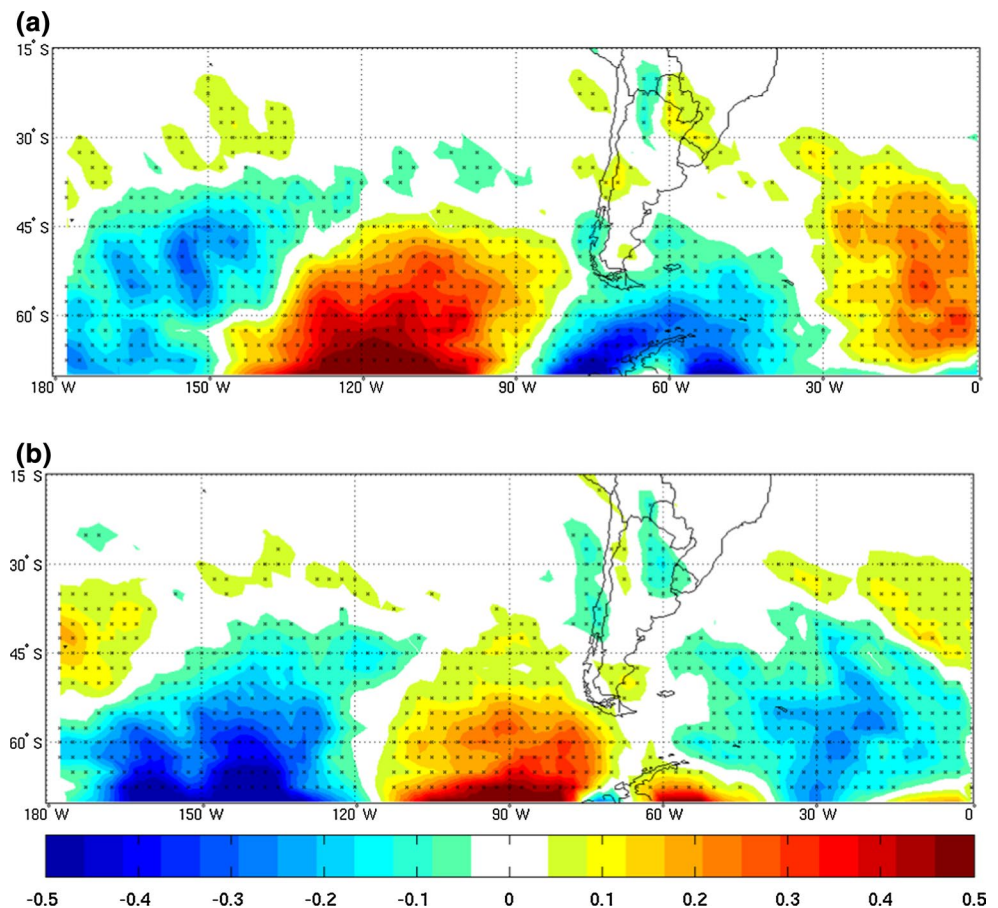


is modulated by the variability of the atmospheric circulation and in turn how the fronts affects the precipitation anomalies at the intraseasonal timescale. The first step is to identify the main modes of variability of the FI on the 11–60 days timescale. Second, the way those modes are conditioned by the intraseasonal variability of the atmospheric circulation (represented by the 500 hPa geopotential height anomalies) is analysed and finally how precipitation anomalies are affected by this relationship it is explored. Accordingly, Fig. 1 displays the regression of the filtered first two principal components (PC) of FI against the FI field over the SH. These two leading modes explain 12.77 % of the total variance (6.57 and 6.20 % the first and second mode, respectively). It can be seen in Fig. 1a that most of the signal in the first mode is located in the southern part of the domain with three well defined centres alternating positive and negative values, all statistically significant with a confidence level of 95 %. One of the centres of action is located in the south-eastern Pacific sector (95°W–65°S). Solman and Orlanski (2010) identified a quasi-stationary high pressure anomaly over the south-eastern Pacific Ocean, which may inhibit the frontal activity, in agreement with the negative FI anomaly displayed in the figure. Fronts that grow up along the Pacific storm-tracks

weaken due to the presence of the high. In fact, the regression of PC1 of FI against the 500 hPa geopotential height anomalies confirms this behaviour (not shown). The second leading mode (Fig. 1b) displays a similar pattern compared with the first one, but in quadrature with the first mode. The regression of PC2 of FI against the 500 hPa geopotential height anomalies (not shown) displays positive height anomalies located where FI anomalies are negative and vice versa. In summary, FI anomalies are anti correlated with 500 hPa height anomalies.

The EOF of the 500 hPa geopotential height anomalies was also calculated in order to analyse the relationship with the frontal activity. The main modes of the intraseasonal 500 hPa geopotential height anomalies (not shown) display the typical structures: the SAM (first mode) and the PSAs (second and third modes, respectively). The regression of the second and third PCs of the 500 hPa geopotential height with the FI anomalies is shown in Fig. 2. It is interesting to note that this Figure is very similar to Fig. 1, suggesting that the modes of variability of FI are conditioned by the variability of the 500 hPa geopotential height field. Comparing Figs. 1 and 2, it is important to note that the second (first) mode of FI variability displayed in Fig. 1b (Fig. 1a) is similar to the regression between the PC associated to

**Fig. 2** Regression of the front-index anomaly field against second (a) and third (b) PCs of 500 hPa geopotential height calculated with the filtered (11–60 days) anomalies. Dots mean 95 % confidence level, according a Fisher test. Units are  $1.e10 \text{ } ^\circ\text{C m}^{-1} \text{ s}^{-1}$





PSA1 (PSA2) with the FI anomalies displayed in Fig. 2a (Fig. 2b but with opposite sign). The result reinforces the control exerted by the variability of the large scale circulation on the variability of the frontal activity. The agreement between the spatial structure of the main modes of variability of FI and the regression between FI anomalies and the PSA modes of 500 hPa geopotential height suggests that the variability of the large scale circulation may exert a control on the variability of the frontal activity, one of the hypothesis posed. The question now is how could the variability of the frontal activity affect the precipitation variability? To explore this relationship, the precipitation anomalies were regressed with the PCs of the FI. Results are shown in Fig. 3. The modes of variability of the FI have associated precipitation anomalies over part of the SH, most of them statistically significant with a confidence level of 95 %. Moreover, the largest precipitation anomalies associated with FI are located over southwestern South America where the FI variability has the largest signal as well. Furthermore, by comparing this figure with Fig. 1 it can be seen that positive (negative) values of the front index anomalies agree with positive (negative) values of precipitation anomalies. As expected, more (less) than average frontal activity leads to more (less) precipitation. Over

the South American continent, Fig. 3 suggests an opposite behaviour of the precipitation anomalies over SESA and Southern Chile (SOCH). In summary, Fig. 3 describes how the variability of the frontal activity impacts on precipitation and thus answers the second question that was posed in the Introduction.

Taking into account that the frontal activity variability is driven by the variability of the atmospheric circulation, hereinafter it could be of interest to check if the relationship between the variability of 500 hPa geopotential height and precipitation has to do with fronts variability. Consequently, Fig. 4 shows the regression of the PC of the 500 hPa geopotential height with precipitation anomalies. It can be seen that the anomalies of precipitation associated with the variability of geopotential height are very similar to those associated with the variability of FI pointing out that the atmospheric circulation variability controls the variability of the frontal activity which affects the precipitation anomaly pattern.

### 3.2 Temporal evolution of main modes of FI

As it was mentioned previously, the modes of variability of the FI on the intraseasonal timescales are in quadrature.

**Fig. 3** Same as Fig. 1 but for the precipitation anomaly field. Dots mean 95 % confidence level, according a Fisher test. Units are  $\text{mm day}^{-1}$

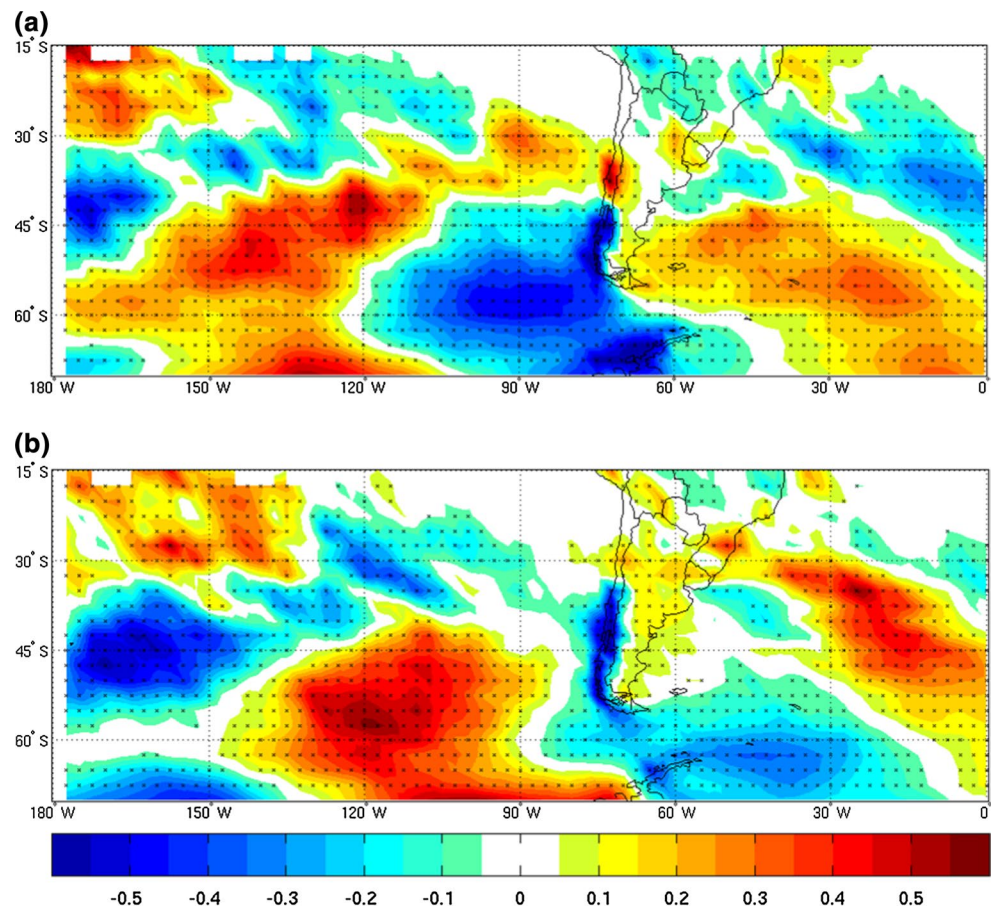


**Fig. 4** Same as Fig. 2 but for the precipitation anomaly field. Dots mean 95 % confidence level, according a Fisher test. Units are  $\text{mm day}^{-1}$

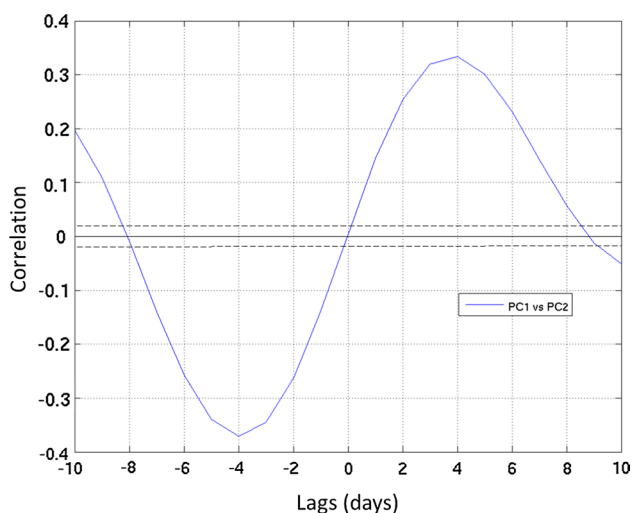
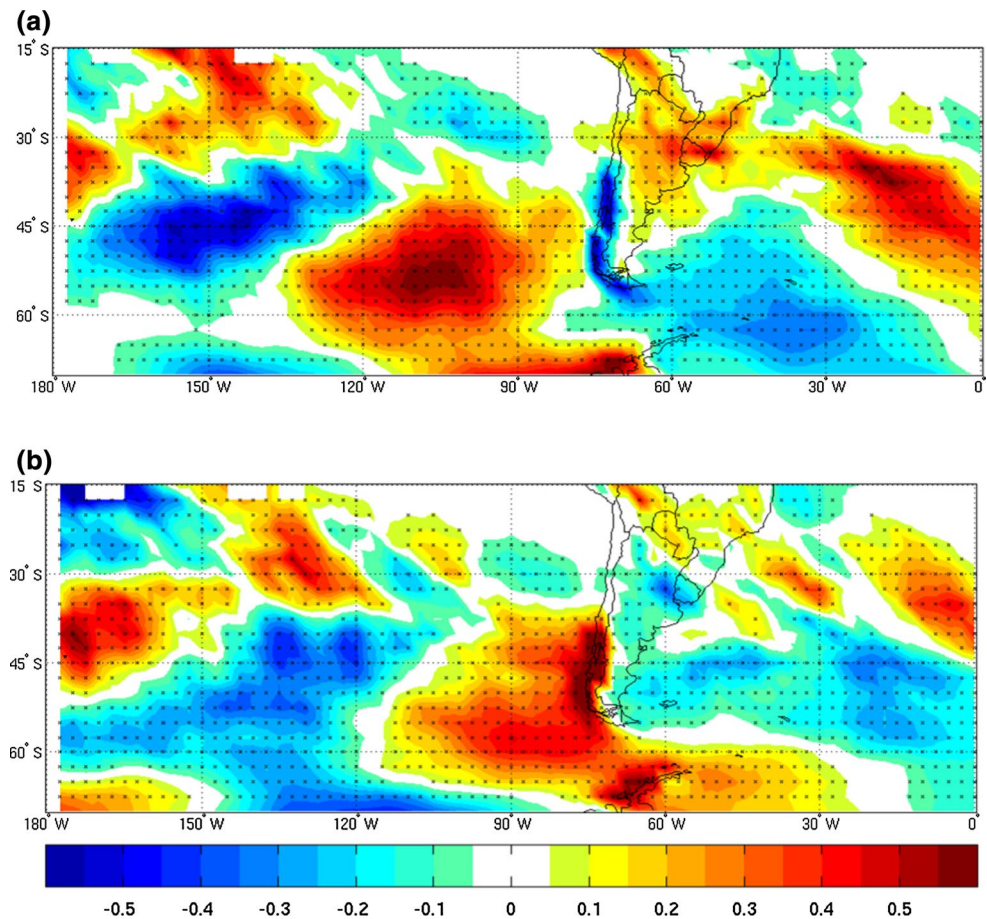


**Fig. 5** Lagged correlation between PC1 and PC2 of front-index. Dash lines indicate 95 % confidence level, according a Fisher test

This could suggest they may be temporally related. In order to explore this behaviour the lagged correlation between PC1 and PC2 of the FI was calculated and it is shown in Fig. 5. It can be seen that effectively the two modes of

variability are related. Moreover, the maximum and minimum correlation coefficients between the two time series are found at lags 4 and  $-4$ , respectively, suggesting a progression of the FI anomalies towards the east. The figure also shows that the period of each mode is approximately 17 days. This behaviour is much related with that found by Mo and Higgins (1998) (hereinafter MH), but for the PCs of PSA1 and PSA2 patterns. It is worth to remind that the atmospheric circulation variability influences the variability of frontal activity, thus the similarity with MH is expected. Moreover, the power spectrum of the PC1 and PC2 of the FI (not shown) display a pick around 17 days, in agreement with results found by MH and by Robertson and Mechoso (2003). The former study identified the PSAs patterns using a 10-days low-pass filtered 200 hPa eddy streamfunction anomaly and found a peak in the spectrum in the band 16–18 days; the second found a peak in 15 days, but for 10-days low-pass filtered anomalies of 700 hPa geopotential height.

The temporal behaviour of the two main modes of FI can be explored in Fig. 6, which shows a lagged regression analysis between FI averaged in a box centred in  $65^{\circ}\text{S}$  and  $95^{\circ}\text{W}$  (hereafter FI95, displayed in Fig. 1) and FI anomaly field. The box for the FI95 time series is



located over the centre of action of the first mode of FI. The regression at lag 0 shows a pattern similar to the first mode of FI (Fig. 1a) but with opposite sign suggesting that the time series of the box FI95 is a good representation of the behaviour of PC1. For lags  $-4$  and  $4$  the pattern is similar to the second mode of FI, while both lags  $-8$  and  $8$  resemble the first mode. The progression from lag  $-8$  to lag  $8$  shows a sequence of the spatial pattern of FI anomaly field, where modes 1 and 2 alternate each approximately 4 days and positive and negative phases of the same mode alternate each 8 days. Note that at lags  $-8$  and  $8$  the pattern is repeated, suggesting that the total cycle is completed in around 17 days. This analysis supports the period of around 17 days of mode 1 discussed above. Moreover, inspection of Hovmöller diagrams of lagged

correlations between the FI95 time series and the FI anomalies averaged over two latitudinal bands ( $65^{\circ}\text{S}$ – $45^{\circ}\text{S}$  and  $70^{\circ}\text{S}$ – $50^{\circ}\text{S}$ , not shown), suggest a wave packet of frontal activity characterized by a downstream development from  $170^{\circ}\text{W}$  to  $20^{\circ}\text{E}$  with a temporal duration of around 16–17 days, in agreement with the behaviour mentioned previously.

To explore how this temporal evolution affects the precipitation anomalies over the SH, a lagged regression analysis was performed between the time series of FI95 and the precipitation anomaly field, displayed in Fig. 7. The first thing to note is the Rossby wave-like pattern in the anomaly precipitation field. At lag 0 it is shown that the precipitation anomalies depict a similar structure to that found in Fig. 3a, but with opposite sign. Furthermore, at lag  $-4$  the pattern is similar to the pattern shown in Fig. 3b. Note that for lags  $-8$  and  $8$  the patterns of precipitation anomalies in the vicinity of the South American continent show a similar structure, suggesting once more a 17-days period in the precipitation anomalies associated with the frontal activity. Moreover Alvarez et al. (2014) also found a 17-days period for the precipitation anomalies over SESA associated with the leading mode of the outgoing long-wave radiation (OLR) at the intraseasonal timescales for winter. Moreover, in Fig. 7, from lag  $-8$  to lag  $8$  it can be distinguished over South America an opposite pattern between SESA and SOCH (Southern Chile). To explore the connexion between these regions, areal average of precipitation over SESA and SOCH were calculated (the boxes corresponding to SESA and SOCH regions are shown in the panel corresponding to lag 0 of Fig. 7). Figure 8 displays the lagged correlation between FI95 and filtered precipitation anomalies in SESA and SOCH. In this case, precipitation anomalies were calculated using CPC-uni data, because the boxes of precipitation are defined over land. It is worth to note that correlation was also done using ERA40 reanalysis and the result was very similar. The first thing to note is that precipitation anomalies associated with the frontal activity over the south-eastern Pacific Ocean in the two regions are in opposite phase, confirming the behaviour shown in Fig. 7. When FI95 is positive there is a maximum correlation with the precipitation anomaly over SOCH and a maximum anticorrelation with precipitation over SESA region at lag 3. This pattern reverses at lag 10. This behaviour suggests that the precipitation anomalies over these two regions are consistent and controlled by the progression of the frontal activity. In order to confirm the behaviour of the pattern of the precipitation anomalies, an EOF analysis was performed on the precipitation anomaly field over southern South America. The first three modes display opposite signs in these regions (not shown) and explain 19 % of the total variance. To further analyse

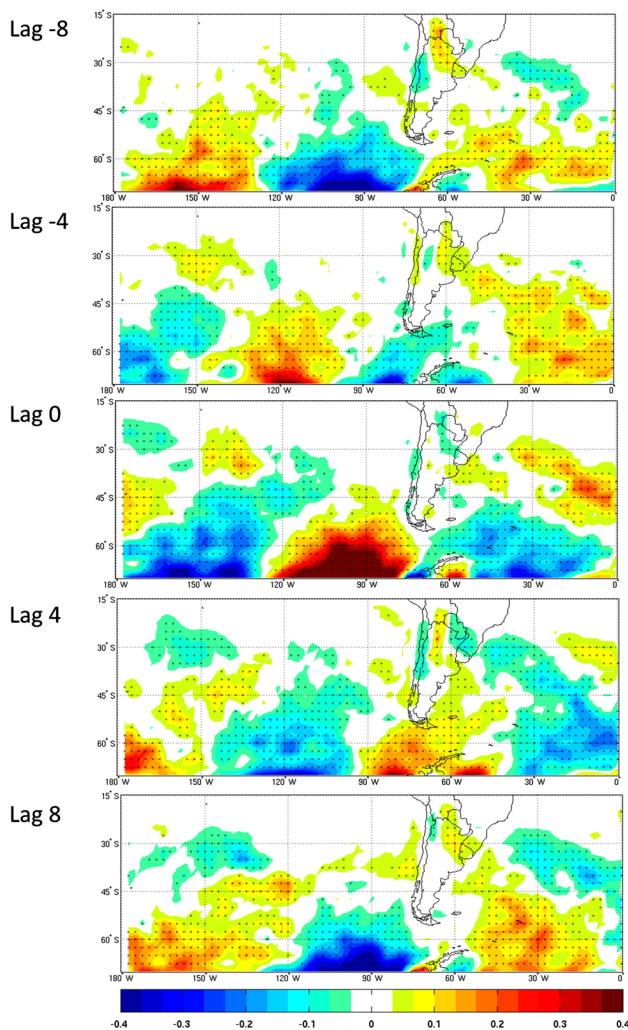


**Fig. 6** Lagged regression of the front-index anomaly field against the filtered (11–60 days) time series of FI95 from lag  $-8$  to 8 days. Dots mean 95 % confidence level, according a Fisher test. Units are  $1.e10\text{ }^{\circ}\text{C m}^{-1}\text{ s}^{-1}$

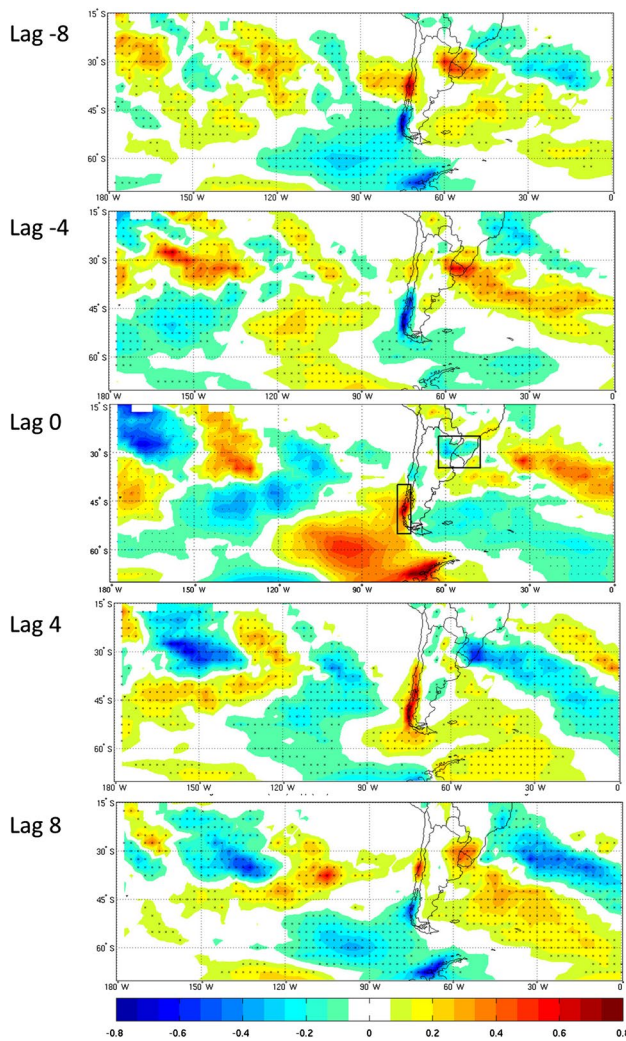


**Fig. 7** Same as Fig. 6 but for the precipitation anomaly field. *Dots* mean 95 % confidence level, according a Fisher test. Units are  $\text{mm day}^{-1}$

the relationship between precipitation anomalies at both SESA and SOCH regions at the intraseasonal timescale, lagged correlations were calculated. Results are shown in Fig. 9. The maximum negative correlation is found in lag 0, indicating that both regions are in opposite phase. Given the evidence discussed previously, this behaviour may be due to the frontal activity. It is worth to note that every 16–17 days the precipitation anomalies in SESA and SOCH are positively correlated, suggesting that positive anomalies over SESA occurs close to 7 days before and 8 days after positive anomalies occur over SOCH. This period matches with that found in Fig. 7, where every 17 days (approximately) the pattern of the precipitation anomalies field influenced by the FI anomaly in FI95 region is repeated.

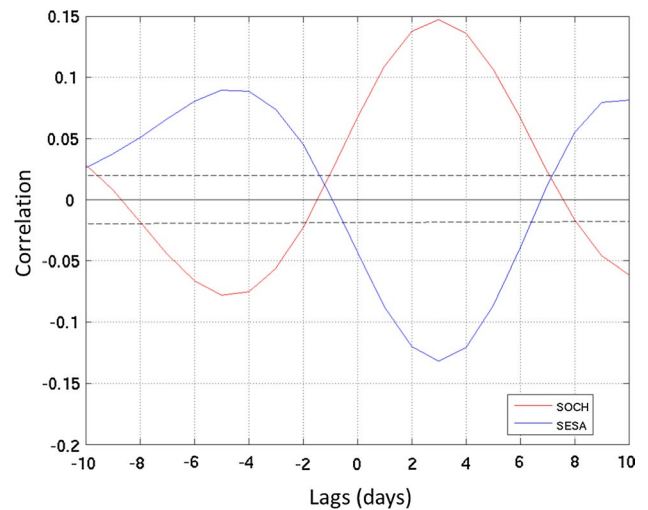


**Fig. 8** Lagged correlation between the filtered (11–60 days) time series of FI95 and time filtered (11–60 days) series of precipitation in SESA (blue line) and SOCH (red line). *Dash lines* indicate 95 % confidence level, according a Fisher test

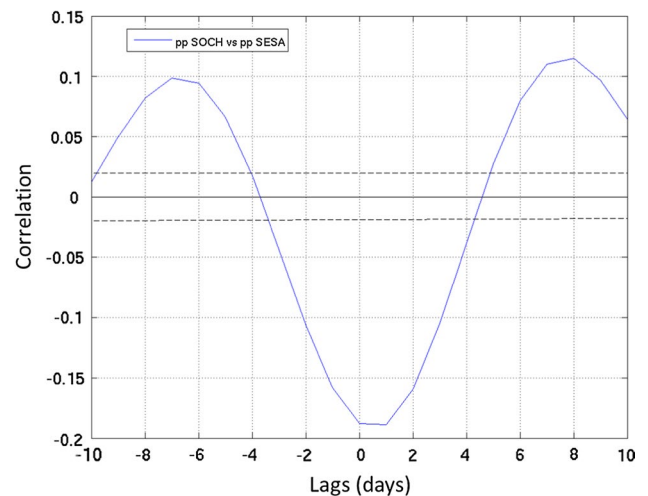


**Fig. 9** Lagged correlation between filtered (11–60 days) time series of precipitation in SOCH and filtered (11–60 days) time series of precipitation in SESA. *Dash lines* indicate 95 % confidence level, according a Fisher test

#### 4 Summary and conclusions

The main objective of this paper is to analyze the variability of the frontal activity in order to better understand its relationship with the large-scale atmospheric circulation and precipitation variability at the intraseasonal timescale (11–60 days). The analysis is focused on the SH winter season, due to wintertime precipitation over subtropical to high latitudes is mostly triggered by fronts (Catto et al. 2012).



The frontal activity is represented by the FI, introduced by Solman and Orlanski (2010) and the 500 hPa geopotential height is used to characterize the large-scale atmospheric circulation. An EOF analysis was applied to the filtered anomalies of FI in order to identify the main patterns of variability at the intraseasonal timescales. The two leading modes of FI showed centers of positive and negative values located over the high latitudes of SH, especially over the southern Pacific Ocean and the south-western Atlantic sector. Moreover, the regression between the PCs of the filtered 500 hPa geopotential height anomaly field (the so-called PSAs modes) and the FI anomaly field shows a pattern which resembles the main modes of variability of FI, suggesting that variability modes of FI are influenced by intraseasonal variability of the large scale circulation, i.e. frontal activity is controlled by the atmospheric circulation. It was also found that precipitation anomalies are affected by the intraseasonal variability of fronts: positive (negative) anomalies of the FI match with positive (negative) anomalies of precipitation, indicating that the variability of fronts impacts on the variability of precipitation. Moreover, precipitation anomalies projected onto PCs of both FI and the 500 hPa showed similar structures. These results may be considered as evidence for supporting the hypothesis posed in the Introduction section: the intraseasonal variability of the frontal activity is influenced by the intraseasonal variability of the atmospheric circulation and in turn affects the variability of precipitation at these timescales.

Furthermore, the two main modes of variability of FI are in quadrature and temporally related. This behavior is supported by a lagged regression analysis showing that the first and second modes alternate each other every 4 days and positive and negative phases of the same mode alternate every 8 days, approximately, suggesting a period of around 17 days. Additionally, the lagged correlation between the PCs of the first and second modes of FI also suggests a 17 days period for each FI mode, agreeing with results found by MH, but for the PCs of PSA1 and PSA2. It was also found that frontal activity develops within a wave-packet characterized by a downstream development with duration of around 16–17 days. The lagged regression between the FI95 time series (calculated as an area average of FI over one of the centers of action) and precipitation anomalies over the SH showed that the precipitation anomaly field associated with frontal activity variability is repeated around every 17-days (especially in the vicinity of South America). This result is in agreement with those found by Alvarez et al. (2014), who identified a 17-days period in the precipitation anomaly field, but regressed against OLR. Inspection of the sequence of regression maps from lags  $-8$  to  $8$ , an opposite pattern between SESA and SOCH regions was found in the precipitation anomaly field. Furthermore, lagged correlation between time series of FI95 and time series of the average

precipitation anomalies in SESA and SOCH confirms the opposite behaviour in both regions. This result suggests that precipitation anomalies over these two regions are controlled by the progression of the frontal activity. This opposite pattern is also appreciated in the correlation between SESA and SOCH, where a maximum negative correlation was found at lag 0, reinforcing that precipitation over these regions is anticorrelated. Moreover, the maximum positive correlation between the two time series repeated every 16–17 days, suggesting that the frontal activity is to a large extent responsible of this behaviour.

Overall this study suggests that the intraseasonal variability of the frontal activity over the SH during wintertime is conditioned by the variability of the atmospheric circulation and in turn modulates the precipitation anomalies at this timescale. Moreover, the 17-days period highlighted in this study associated with the evolution of the frontal activity wave-packet, may be useful for extended range prediction of precipitation anomalies in the region.

From these results and taking into account the numerous articles that relate the atmospheric circulation and precipitation anomalies at the interannual timescales, this study will be extended to better understand to what extent the interannual variability of fronts may relate with the interannual variability of precipitation over the SH.

**Acknowledgments** The authors are grateful to Dr. Isidoro Orlanski for his insightful comments and suggestions on the manuscript. The authors also thank to two anonymous reviewers for their valuable comments that helped to improve this paper. This work was supported by the following grants: FONCyT—PICT-2012-1972, PIP-CONICET No. 112-201101-00189 and UBACYT2014 No. 20020130200233BA.

## References

- Alvarez MS, Vera CS, Kiladis GN, Liebmann B (2014) Intraseasonal variability in South America during the cold season. *Clim Dyn* 42:3253–3269. doi:[10.1007/s00382-013-1872-z](https://doi.org/10.1007/s00382-013-1872-z)
- Berbery EH, Vera CS (1996) Characteristics of the Southern Hemisphere storm track with filtered and unfiltered data. *J Atmos Sci* 53:468–481. doi:[10.1175/1520-0469\(1996\)053<0468:COTSHW>2.0.CO;2](https://doi.org/10.1175/1520-0469(1996)053<0468:COTSHW>2.0.CO;2)
- Bjerknes J, Solberg H (1922) Life cycle of cyclones and the polar front theory of atmospheric circulation. *Geophysisks Publikationer* 3:1–18
- Browning KA, Roberts NM (1994) Structure of a frontal cyclone. *Q J R Meteorol Soc* 120:1535–1557. doi:[10.1002/qj.49712052006](https://doi.org/10.1002/qj.49712052006)
- Catto JL, Jakob C, Berry G, Nicholls N (2012) Relating global precipitation to atmospheric fronts. *Geophys Res Lett* 39:L10805. doi:[10.1029/2012GL051736](https://doi.org/10.1029/2012GL051736)
- Cavalcanti IFA, Kayano MT (1999) High-frequency patterns of the atmospheric circulation over the Southern Hemisphere and South America. *Meteorol Atmos Phys* 69:179–193. doi:[10.1007/BF01030420](https://doi.org/10.1007/BF01030420)
- Cunningham CAC, Cavalcanti IFA (2006) Intraseasonal modes of variability affecting the South Atlantic Convergence Zone. *Int J Climatol* 26:1165–1180. doi:[10.1002/joc.1309](https://doi.org/10.1002/joc.1309)

- Duchon CE (1979) Lanczos filtering in one and two dimensions. *J Appl Meteorol* 18:1016–1022. doi:[10.1175/1520-0450\(1979\)018<1016:LFIQAT>2.0.CO;2](https://doi.org/10.1175/1520-0450(1979)018<1016:LFIQAT>2.0.CO;2)
- Ghil M, Mo K (1991) Intraseasonal oscillations in the global atmosphere. Part II: Southern Hemisphere. *J Atmos Sci* 48:780–790. doi:[10.1175/1520-0469\(1991\)048<0780:IOITGA>2.0.CO;2](https://doi.org/10.1175/1520-0469(1991)048<0780:IOITGA>2.0.CO;2)
- Gonzalez PLM, Vera C (2014) Summer precipitation variability over South America on long and short intraseasonal timescales. *Clim Dyn* 43:1993–2007. doi:[10.1007/s00382-013-2023-2](https://doi.org/10.1007/s00382-013-2023-2)
- Hannachi A, Jolliffe IT, Stephenson DB (2007) Empirical orthogonal functions and related techniques in atmospheric science: a review. *Int J Climatol* 27:1119–1152. doi:[10.1002/joc.1499](https://doi.org/10.1002/joc.1499)
- Kidson JW (1988) Indices of the Southern Hemisphere zonal wind. *J Clim* 1:183–194. doi:[10.1175/1520-0442\(1988\)001<0183:IOTSHZ>2.0.CO;2](https://doi.org/10.1175/1520-0442(1988)001<0183:IOTSHZ>2.0.CO;2)
- Kidson JW, Sinclair MS (1995) The influence of persistent anomalies on Southern Hemisphere storm tracks. *J Clim* 8:1938–1950. doi:[10.1175/1520-0442\(1995\)008<1938:TIOPAO>2.0.CO;2](https://doi.org/10.1175/1520-0442(1995)008<1938:TIOPAO>2.0.CO;2)
- Liebmann B, Kiladis GN, Marengo JA, Ambrizzi T, Glick JD (1999) Submonthly convective variability over South America and the South Atlantic Convergence Zone. *J Clim* 12:1877–1891. doi:[10.1175/1520-0442\(1999\)012<1877:SCVOSA>2.0.CO;2](https://doi.org/10.1175/1520-0442(1999)012<1877:SCVOSA>2.0.CO;2)
- Mo KC, Ghil M (1987) Statistics and dynamics of persistent anomalies. *J Atmos Sci* 44:877–902. doi:[10.1175/1520-0469\(1987\)044<0877:SADOPA>2.0.CO;2](https://doi.org/10.1175/1520-0469(1987)044<0877:SADOPA>2.0.CO;2)
- Mo KC, Higgins RW (1998) The Pacific–South American modes and tropical convection during the Southern Hemisphere winter. *Mon Weather Rev* 126:1581–1596. doi:[10.1175/1520-0493\(1998\)126<1581:TPSAMA>2.0.CO;2](https://doi.org/10.1175/1520-0493(1998)126<1581:TPSAMA>2.0.CO;2)
- Nogués-Paegle J, Mo KC (1997) Alternating wet and dry conditions over South America during summer. *Mon Weather Rev* 125:279–291. doi:[10.1175/1520-0493\(1997\)125<0279:AWADCO>2.0.CO;2](https://doi.org/10.1175/1520-0493(1997)125<0279:AWADCO>2.0.CO;2)
- Pook MJ, McIntosh PC, Meyers GA (2006) The synoptic decomposition of cool-season rainfall in the southeastern Australian cropping region. *J Appl Meteorol Climatol* 45:1156–1170. doi:[10.1175/JAM2394.1](https://doi.org/10.1175/JAM2394.1)
- Richman MB (1986) Rotation of principal components. *J Climatol* 6:293–335
- Robertson AW, Mechoso CR (2003) Circulation regimes and low-frequency oscillations in the South Pacific sector. *Mon Weather Rev* 131:1566–1576. doi:[10.1175//2548.1](https://doi.org/10.1175//2548.1)
- Solman SA, Orlanski I (2010) Subpolar high anomaly preconditioning precipitation over South America. *J Atmos Sci* 67:1526–1542. doi:[10.1175/2009JAS3309.1](https://doi.org/10.1175/2009JAS3309.1)
- Solman SA, Orlanski I (2014) Poleward shift and change of the frontal activity in the Southern Hemisphere over the last 40 years. *J Atmos Sci* 71:539–552. doi:[10.1175/JAS-D-13-0105.1](https://doi.org/10.1175/JAS-D-13-0105.1)
- Thompson DWJ, Wallace JM (2000) Annular modes in the extratropical circulation. Part I: month-to-month variability. *J Clim* 13:1000–1016. doi:[10.1175/1520-0442\(2000\)013<1000:AMITEC>2.0.CO;2](https://doi.org/10.1175/1520-0442(2000)013<1000:AMITEC>2.0.CO;2)
- Uppala SM et al (2005) The ERA-40 re-analysis. *Q J R Meteorol Soc* 131:2961–3012. doi:[10.1256/qj.04.176](https://doi.org/10.1256/qj.04.176)
- Vera C (2003) Interannual and interdecadal variability of atmospheric synoptic-scale activity in the Southern Hemisphere. *J Geophys Res* 108(C4):8077. doi:[10.1029/2000JC000406](https://doi.org/10.1029/2000JC000406)
- Xie P, Chen M, Yang S, Yatagai A, Hayasaka T, Fukushima Y, Liu C (2007) A gauge-based analysis of daily precipitation over East Asia. *J Hydrometeorol* 8:607–626. doi:[10.1175/JHM583.1](https://doi.org/10.1175/JHM583.1)